Handheld LIBS analysis for in situ quantification of Li and detection of the trace elements (Be, Rb and Cs)

Cécile Fabre, Nour Eddine Ourti, Christophe Ballouard, Julien Mercadier, Jean Cauzid

Handheld LIBS analysis for *in situ* quantification of Li and detection of the trace elements (Be, Rb and Cs)

Cécile Fabre[1]*, Nour Eddine Ourti[1], Christophe Ballouard[1], Julien Mercadier[1], Jean Cauzid[1]

[1]GeoRessources CNRS-Université de Lorraine,
BP 70239, 54506 Vandoeuvre-les-Nancy, France

* cecile.fabre@univ-lorraine.fr

Abstract

The world's lithium demand is currently increasing due to its use in batteries and in green energy technologies. As a consequence, Li has recently been added to the list of critical materials in Europe. Finding new deposits is necessary in order to guarantee a mid- to long-term stable supply. Granites and associated pegmatites are the primary 'hard-rock' source for Li, where it is present in a variety of aluminosilicate minerals. Li is a light element that typically occurs at low concentrations in rocks and minerals, which presents challenges for some analytical techniques (e.g., portable X-ray fluorescence) for exploration. Laser induced breakdown spectroscopy (LIBS) is a powerful analytical technique for the acquisition of simultaneous almost all elements of the periodic table. LIBS has particular sensitivity to the light elements (Z<13) and, therefore, handheld LIBS has significant potential for the exploration of pegmatite- or granite-related Li mineralization. For this study, a suite of 16 pegmatite-hosted Li ore minerals comprising the three main aluminosilicate species (spodumene, lepidolite and petalite) that contained between 1.36 to 3.54 wt.% Li was analyzed using a handheld LIBS instrument. A univariate calibration curve was developed for LIBS quantification of Li in these minerals using the strong Li emission lines at 610.36 nm and 670.79 nm (R^2 >0.9, RMSD = 0.2 wt. % Li). Simultaneous quantification of Li contents and measurement of major element ratios (e.g., Si/Al) using portable LIBS permits rapid discrimination between different Li-bearing silicates, such as spodumene and petalite, that can be difficult to identify in the field on the basis of macroscopic criteria. Moreover, the detection of minor/trace elements such as Be, Rb and Cs is possible by handheld LIBS, which can provide useful information for rare metal pegmatite and granite exploration. Thus, qualitative and quantitative analysis by handheld LIBS represents a very promising approach for Li exploration.

Keywords: LIBS, lithium, Li minerals, handheld analysis

1. Introduction

The economic importance of Li is growing as it represents a key component in the manufacturing of green energy storage-devices such as Li-ion batteries (Bibienne et al., 2020). As consequence, the global demand for Li has recently increased and Li was officially added in 2020 to the list of critical raw materials published by the European Commission for the European Union (COM-2020-474). Most Li resources around the world are hosted in brine deposits from salars or geothermal fields, but other important sources are volcanic-sedimentary clays, granites, and granite-related pegmatites (Kesler et al., 2012; Bowell et al., 2020). Although salar deposits contain the largest Li reserve, Li-rich mineral concentrates from pegmatites are currently the main source of Li production due to its higher grade and lower production cost (Bowell et al., 2020). As previously described by various authors (Černý, 1991; Defnet et al., 2021; London, 2014, 2005a) the granite-associated pegmatites that are sources of rare metals belong to two very distinct families - the Li–Cs–Ta (LCT) pegmatites and the Nb–Y–F (NYF) pegmatites. Quartz, potassium feldspar, and albite are the major constituents in both the LCT and NYF pegmatites, with muscovite, biotite, garnet, tourmaline, and apatite typically present as accessory phases. Pegmatites of the LCT family are characterized by enrichment in Li, Rb, Cs, Be, Sn, Nb, Ta, B, P and F (Barros et al., 2020; London, 2014, 2005b). Most LCT pegmatites occur worldwide in supracrustal rocks metamorphosed in the upper greenschist to lower amphibolite facies that are are typically located in the vicinity of evolved, S-type peraluminous granites and leucogranites from which they are inferred to be derived by fractional crystallization . In chemically evolved LCT pegmatites, spodumene, petalite, and lepidolite are the major Li-bearing minerals. Beryl is the primary host mineral for Be, pollucite for Cs, the columbite group minerals for Nb and Ta, and cassiterite for Sn. Exploration and assessment for LCT pegmatites are guided by a number of observations that include increasing contents of Li in white mica and increasing Mn in garnet (Charoy et al., 1995). Thus, pegmatite- or granite-hosted Li mineralization is characterized by a wide geographic distribution and the generation of valuable byproducts that include other strategic rare metals such as Ta, Nb, Sn, Be, Cs, and Rb as well as raw materials such as quartz, feldspar, and micas (Defnet et al., 2021; Kesler et al., 2012; Linnen et al., 2012). As suggested by London (London, 1984), "… the lithium aluminosilicate phase diagram constitutes a petrogenetic grid from which P-T

conditions of emplacement and crystallization can be ascertained for many lithium alumino silicate-bearing pegmatites".

In western Europe, such 'hard-rock' Li deposits, which offer the best potential to supply the continent for the immediate future (Gourcerol et al., 2019), are primarily associated with rare-metal granites and pegmatites of the Variscan orogenic belt that extends for more than 3,000 km from southwestern England, through Spain, France, and Germany to the Czech Republic. Typical Li ore minerals include aluminosilicate phases, such as spodumene, petalite, micas (e.g., lepidolite), and phosphate minerals (e.g., montebrasite) that are disseminated within granite and localized in associated pegmatite bodies and local metasomatic greisens. The typically small size of these intrusions (generally <1 km^3), together with the absence of petrophysical characteristics of mineralization, are serious limitations for exploration. Moreover, due to its small atomic weight, Li cannot be detected by X-ray fluorescence (XRF) spectrometry so that the handheld XRF analyzers commonly used during field exploration campaigns for metal deposits cannot be used for identifying Li mineralization.

This work is part of LIGHTS (Lightweight Integrated Ground and Airborne Hyperspectraln Topological Solution), a European research project aimed at improving techniques for Li exploration, including the evaluation of portable tools. Our objective was to use handled laser-induced breakdown spectroscopy (LIBS) to identify and discriminate between the Li-bearing phases spodumene, petalite, and lepitolite commonly encountered in metallogenic provinces associated with rare-metal pegmatites and granites and to quantify their Li contents by developing a calibration curve for these minerals. Some minerals are quite difficult to distinguish in the field due to their similar colors (see Supp. Figures S1a, S1b and S1c). We aimed to establish the LIBS calibration curve of Li content for different matrices. We also assess the potential of using handheld LIBS to check the Al/Si emission line ratios to discriminate between these Li minerals, as well as for the detection of other rare metals such as Be, Cs and Rb that can be directly mined along with Li or be used as exploration vectors for Li-mineralization.

2. Background

Details of the LIBS technique have been described in several reviews (Cremers and Radziemski, 2006; Hahn and Omenetto, n.d.; Radziemski and Cremers, 2013; Senesi, 2014; Fabre, 2020; Harmon and Senesi, 2021; Senesi et al., 2021). The components of a typical LIBS

system are basically the laser source (typically a Q-switched Nd:YAG at 1064 nm), a gated detector attached to the spectrograph/spectrometer array, fiber optic cable that allows energy transit from the laser source to the sample, and a detector that is sensitive to the plasma-related emissions. LIBS has been attracting the interest of the scientific community over the past 50 years, which generated significant technical improvements especially during the last two decades as a consequence of the miniaturization of the component lasers, spectrometers, computers, and electronics along with an increase in the storage capacity of the batteries powering the devices. Multiple prototypes of field-portable LIBS systems were developed during the 1990s that were (i) lightweight to provide maneuverability for field-use, (ii) solid and ruggedized for use under different field-conditions, (iii) simple to use, and (iv) optimized for the detection of a large number of elements over a minimal acquisition time (Connors et al., 2016; Cuñat et al., 2005; Palanco et al., 2003; Rakovský et al., 2014). This work led to the more recent development and marketing of commercial handheld LIBS analyzers by multiple manufacturers. Several recent studies describe the use of handheld LIBS for different geological applications that include mineral exploration (Connors et al., 2016; Defnet et al., 2021; Harmon et al., 2019, 2021; Lawley et al., 2021; Senesi, 2014; Senesi et al., 2021).

Lithium is an important geochemical tracer for fluids or solids, but its abundance variation at the micrometer scale is not readily determined through most analytical techniques and its bulk concentration can only be measured using classical bulk analytical techniques. Although a scanning electronic microprobe fitted with a soft X-ray emission spectrometer (SXES) can analyze for Li at high spatial resolution (Takahashi et al., 2015), this is an expensive and time-consuming analytical procedure that can only be undertaken in the laboratory. Not only is LIBS one of the few analytical techniques for rapid Li detection down to the ppm level (Fabre et al., 2021, 2002) it is one that can be employed outside the laboratory in the field. Thus, the analysis of Li using LIBS has been the subject of geological interest (Fabre et al., 2021, 2002, 1999; Sweetapple and Tassios, 2015; Verlaguet et al., 2016). Fabre et al. (Fabre et al., 2002) used a univariate calibration model for Li quantification in synthetic glasses and natural Li-rich minerals using the characteristic Li line at 670.79 nm and then determined the Li contents of geological materials that included spodumene, petalite, and fine-grained eucryptite from granite pegmatite dikes in Portugal, melt inclusions from the Streltsovka uranium deposit in Siberia, and as a trace element in barren quartz veins from Spain. Estimated wt. % contents of Li in spodumene and petalite Li compared well with abundances obtained from ion microprobe analysis, with the possible exception of eucryptite because its grain size was smaller than the

laser spot size. Since then, numerous studies described the use of LIBS for analysis of silicate gem minerals or other applications in geology (Harmon et al., 2009, 2006; Kochelek et al., 2015; McMillan et al., 2018). For example, Rossi et al. (Rossi et al., 2014) reported Be and B concentrations within gem-quality spodumene, topaz, and tourmaline that were in excellent agreement with LA-ICP-MS and EMPA analyses for the same samples. A LIBS study of spodumene by Sweetapple and Tassios (Sweetapple and Tassios, 2015) showed that it was possible to measure Li, Be, and B in a hydrothermally altered pegmatite, with microscale mapping of Li used to discriminate between spodumene, its alteration mineralogy, and matrix silicates. More recently, new studies have been done combining handheld LIBS tool and geochemical exploration for elemental mapping in Li-rich rocks (Harmon et al., 2021; Lawley et al., 2021).

This study of handheld LIBS analysis had two objectives, to obtain rapid discrimination of Li-rich minerals that are often difficult to distinguish visually in the field and to perform Li quantification beforehand in the laboratory in order to subsequently apply the Li calibration to pegmatite outcrops in the field for the LIGHTS project (Fabre et al., 2021). One of the objectives of this study is then the access to fast and *in situ* use of internal calibration and then reduce at maximum any other use of external treatment of the data. All of the LIBS spectra (each individual LIBS spectra and mean spectra) and more information about the sample analyses or location used in this paper are archived for open access at https://doi.org/10.24396/ORDAR-65.

3. Samples and methods

3.1 Li-bearing samples selection and bulk analyses

There are more than a hundred lithium-bearing minerals, most of which are silicates (Grew, 2020). The most common and economically significant Li bearing minerals are the aluminosilicates present in rare-metal pegmatites and granites, namely spodumene - $LiAlSi_2O_6$, petalite - $LiAlSi_4O_{10}$, and lepidolite - $KLi_2AlSi_4O_{10}F_2$ (Table 1). Other Li-bearing minerals are phosphates, such as montebrasite, amblygonite, and the rarely encountered lithiophosphates. Li contents are the higher in the phosphate minerals, but these are rarely of economic importance (Gourcerol et al., 2019; Kesler et al., 2012). Therefore, this study focused on the Li-bearing silicate minerals, although geological information such as location, mineralogy and Li contents, continuity and size and relation to enclosing rocks, is relatively sparse and scattered (Gourcerol et al., 2019; Kesler et al., 2012; Tadesse et al., 2019).

Table 1

Characteristic of the most common Li-bearing minerals found in economic granite- or pegmatite-related Li deposits. Li wt. % is based on stoichiometry.

Mineral Name	**Mineral Group**	**Chemical Formula**	**Theoretical Li content (wt. %)**
Spodumene	Inosilicate (pyroxene)	$LiAlSi_2O_6$	3-7
Lepidolite	Phyllosilicate (mica)	$K_2(Li,Al)_{5-6}(Si_{6-7}Al_{2-1}O_{20})(OH,F)_4$	1.4 to 3.6
Petalite	Phyllosilicate	$LiAlSi_4O_{10}$	1.6 to 2.3
Amblygonite/ Montebrasite	Phosphate	$LiAl(PO_4)(F,OH)$	3.4 to 4.7
Hectorite	Phyllosilicate (clay mineral)	$Na_{0-3}(Mg,Li)_3Si_4O_{10}(OH)_2$	0.54
Jadarite	Nesosilicate	$LiNaSiB_3O_7(OH)$	7.3

Sixteen large (>2 cm) and visually homogeneous pegmatite-hosted samples of spodumene (n = 9), petalite (n = 4) and lepidolite (n = 3) were selected for our study. The samples were cut in half using a diamond saw. One half with a flat surface was retained for LIBS analyses and the other half was crushed using an agate mortar to obtain a powder fraction for independent chemical analysis. These powders were analyzed at the SARM laboratory (CRPG-CNRS, Nancy, France) using inductively coupled plasma atomic emission spectroscopy (ICP-AES) for major-element analysis, ICP-MS for trace-element analysis, and flame atomic absorption spectrometry (AAS) for Li analysis. Bulk mineral geochemical compositions are provided in Table S1, and the Li contents, which may differ from the theoretical values, are reported in Table 2, and location information of the samples and their structural formulae. Measured bulk concentrations were used as reference concentrations to be compared to the LIBS analyses undertaken on the second sample piece.

Table 2

Mineralogy, provenance and measured Li contents of the samples (AAS). The error obtained for the Li content is 5% (relative percentage)

Sample ID	Mineral	Country of Origin	Li content (wt. %)
Kun-Afg	Kunzite (Spodumene)	Afghanistan	3.54
Spo-Kok	Spodumene	South Africa Namaqualand- Kokerboomrand I	3.31
Spo-Lac	Spodumene	Canada	2.83
Hid-Afg	Hiddenite (Spodumene)	Afghanistan	3.36
Spo-Nor	Spodumene	South Africa Namaqualand-Norabees I	3.25
Spo-Big	Spodumene	Canada/Big Lake	3.17
Spo-Boa	Spodumene	Boa Vista, Portugal	3.46
Spo-Pak	Spodumene	Pakistan	3.36
Spo-Zai	Spodumene	Zaire	1.33
Pet-Bik2	Petalite	Zimbabwe/Bikita	2.04
Pet-Bik	Petalite	Zimbabwe/Bikita	2.16
Pet-Big	Petalite	Canada/Big Lake	2.01
Pet-Tan	Petalite	Canada/Tanco	2.18
Lep-Moz	Lepidolite	Mozambique	2.57
Lep-Cun	Lepidolite	Mauritania	3.02
Lep-Pak	Lepidolite	Pakistan	2.47

As illustrated by the pictures of typical Li minerals shown in a Figure S1, the appearance of these minerals cannot be used for discrimination, as color varies varied from translucent to white, with some brown to pink variants. In order to avoid any bias in the analysis and to obtain the best estimate of Li content, the selection of samples was done on the basis of their visual homogeneity, which may be an indication of uniform composition. As the lepidolite micas have a sheet-like structure, it was not necessary to cut these samples to obtain a flat surface for the LIBS analysis.

3.2 LIBS technique and protocol of analysis

The handheld LIBS analyzer used exclusively for this study was a SciAps model Z-300 analyzer that utilizes a 1064 nm laser source featuring a 5-6 mJ/pulse and 10Hz/50 Hz repetition rate. This instrument has three charge coupled diode (CCD) spectrometers that cover a broad spectral range from 190-950 nm, which permits the detection of one or more emission lines for elements of interest from the ultraviolet (UV) to visible and near-infrared (VNIR)

204 portions of the electromagnetic spectrum. The LIBS analysis has been also done under a
205 constant flux of Ar gas, with the canister, in order to confine the plasma emission and
206 increase its intensity. The analyzer is configured to permit rastering of the laser beam across a 2
207 mm segment of sample and the pattern of the raster grid can be configured to optimize the
208 number of laser points on the sample surface. The number of laser shots can be adjusted to
209 include a few "cleaning" shots prior to data acquisition if dust or an environmental stain is
210 present on the sample. In the case of a surface coating, a LIBS-depth profile can be acquired by
211 taking a number of additional laser shots at any location. These specific characteristics of
212 LIBS analysis are of particular relevance for in situ geologic analysis and exploration
213 application when a presence of coating is suspected. The data acquisition processes described
214 above have be modified for different minerals depending on a sample's physical character and
215 size. For this study, the LIBS raster was acquired generally along a 3x5 point grid with four
216 laser shots for data acquisition made at each point following one cleaning shot. This rater grid
217 was duplicated on each sample and the 30 averaged LIBS spectra from the four laser shots
218 were aggregated to emulate a bulk analysis (Fig. 1).
219 Here, concerning the temporal conditions of the plasma analysis, the delay time was fixed as
220 following: the beginning of the acquisition of the LIBS emission is 400 ns and the acquisition
221 time window is fixed to 1 ms.
222

Fig. 1 Schematic representation of the LIBS analysis for this study illustrating the two 3x5 raster grids that comprised of 15 points of laser spot size of 50 µm in diameter at a 12.5µ spacing.

3.3 Data processing

As noted above, LIBS spectra were acquired over the broad spectral range from 190-950 nm. The maximum emission intensity observed was typically around 30,000 a.u. (arbitrary units) due to the strong Li emission. Emission line selection is the first step in LIBS spectral data processing. In the case of Li, few electronic transitions are possible, which limits the number of emission lines present in a LIBS spectrum. The strongest lines are those at 610.36 nm, 670.79 nm and 812.64 nm. For this study, only the lines at 610.36 nm and the 670.79 nm were used, as these lines exhibited the best signal to noise ratio, displayed simple Voigt profiles, and had no interferences with other peaks (Fig. 2). As the minerals in our study are not Ca-rich (Guezenoc et al., 2019b), the strong interference by the Ca line at 610.23 nm was not observed. Spectra can be exported from the instrument either as individual raw spectral or as averaged spectra, with both options explored in this study. Even if the spectra, which are calibrated in

wavelength, are minimally processed after acquisition by the internal software of the analyzer, these spectra can be used for elemental detection (such as the identification of Be and Cs) or for developing a calibration curve. Examples of mean LIBS spectra for the petalite, spodumene and lepidote minerals, in the UV, VIS and VNIR ranges, are reported in the supplementary figures (S2, S3 and S4).

Concentration estimation by calibration curves is one of the most common aspects of LIBS spectral analysis. This approach to quantification is quite sensitive and depends strongly on the analysis protocol and data processing (Babos et al., 2019; Bennett et al., 2018; Fabre et al., 2014, 2011). The information required for calibration curve development is the total area under a peak, also referred as the LIBS area intensity, which is expressed by the analyzer in arbitrary units (a.u.).

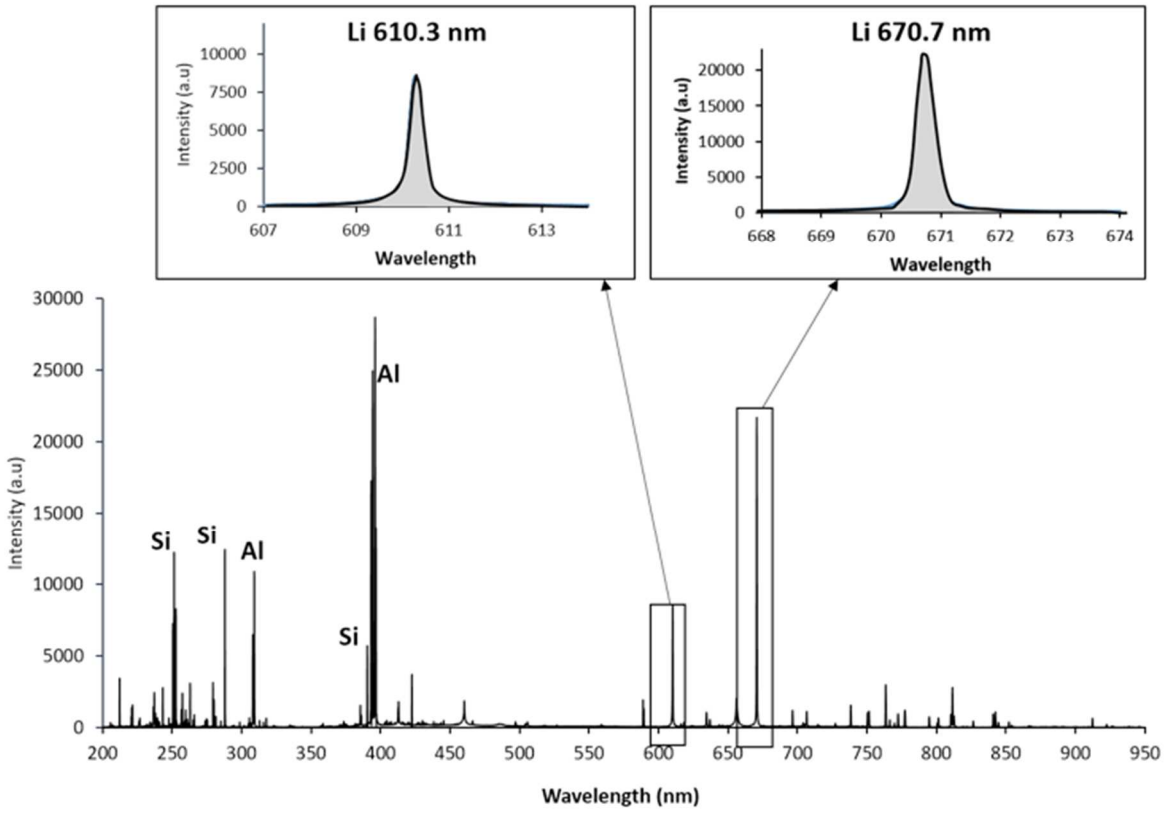

Fig. 2 Averaged LIBS spectrum obtained from analysis of 30 points on a spodumene sample with blowups presented for the two main Li lines (610.36 and 610.79 nm) that were used for the development of the calibration curve for estimation of Li concentrations. The grey area corresponds to the value used for the calibration.

4. Results

4.1 Univariate calibration curve

In order to evaluate the accuracy of our calibration model for Li, figures of merit were calculated according to Equations 1 and 2. These are the root mean squared error of prediction (RMSE-P) and the squared multiple correlation coefficient (R^2). RMSE is a commonly used statistical parameter to compare different models with similar analytical conditions and for a particular variable, as it is scale dependent. In case of linear regression, RMSE provides an indication of accuracy in the model, translating the standard deviation of prediction errors to evaluate the degree of data concentration around the line of best fit. R^2 is also called the "coefficient of determination" and is an indicator of the linear relationship between the X and Y variables, an R^2 value close to 1 indicates a good degree of fit.

$$\mathrm{RMSE-P} = \sqrt{\frac{1}{n}\sum_{i=1}^{n}(y_{pred} - y_{ref})^2} \qquad \text{Equation 1}$$

$$R^2 = \frac{\sum_i (y_{pred} - y_m)^2}{\sum_i (y_{ref} - y_m)^2} \qquad \text{Equation 2}$$

The term y_{pred} is the predicted value from the calibration model, y_{ref} is the reference value from bulk analysis, and y_m is the mean value of the predictors. As recently recalled (Duponchel et al., 2020), a univariate calibration curve is the graphical display of a regression model in which two variables of the same statistical weight are plotted against each other to evaluate the relationship (i.e. correlation) between them. The situation where more than one X variable is simultaneously used to forecast a single dependent Y variable (or vice versa) is a multivariate model. The calibration curve approach used for this study was the univariate model, where X corresponds to the emission area of a selected Li peak in the LIBS spectrum and Y to the independently determined wt. % Li concentration in a sample.

4.2 Lithium calibration on Li minerals

Calibration curves can be developed internally on the Z-300 using its proprietary *Profile Builder* software based on the selection of different element emission peaks, which may be used as collected or after normalization of a spectrum to its entire intensity or through the standard normal variation (SNV) method. This is common practice when analyzing different types of minerals by LIBS to ameliorate potential matrix effects resulting from difference in physical character such as surface texture and hardness (El Haddad et al., 2014; Guezenoc et al., 2019a; Zorov et al., 2010). For this study, total peak areas for both the 610.36 nm and 670.79

nm Li spectral lines were extracted and normalized to the entire LIBS spectra. Spectral normalization is a part of the onboard software of the analyzer that can be selected by the analyst. This may not have been necessary for the hard minerals spodumene and petalite, but it should improve the results as the mica lepidolite displays a very different surface texture and hardness. The *Profile Builder* software first associates with each standard or sample its actual bulk Li content. The total area under a selected Li peak was determined from the 30 averaged analyses, with each sample analyzed across the two 3x5 shot grids. The calibration curve was obtained by taking the area under the curve for each Li peak in the LIBS spectrum and dividing this by the area under the entire LIBS spectrum. Other elements can be added by developing multiple calibration models. This calibration curve is automatically saved in memory and is made available for subsequent analyses on the field. Fig. 3 presents the lithium calibration curve obtained for our suite of 16 Li minerals using the two major Li emission lines. The Y error bars in the figure correspond to the error value derived from bulk chemical analysis of the second piece of each sample, calculated from the flame AAS analyses. This value is a specific function of the Li content of the sample (around 5% relative percentage). The X error bars correspond to the standard error obtained for the 30 averaged spectra for each sample.

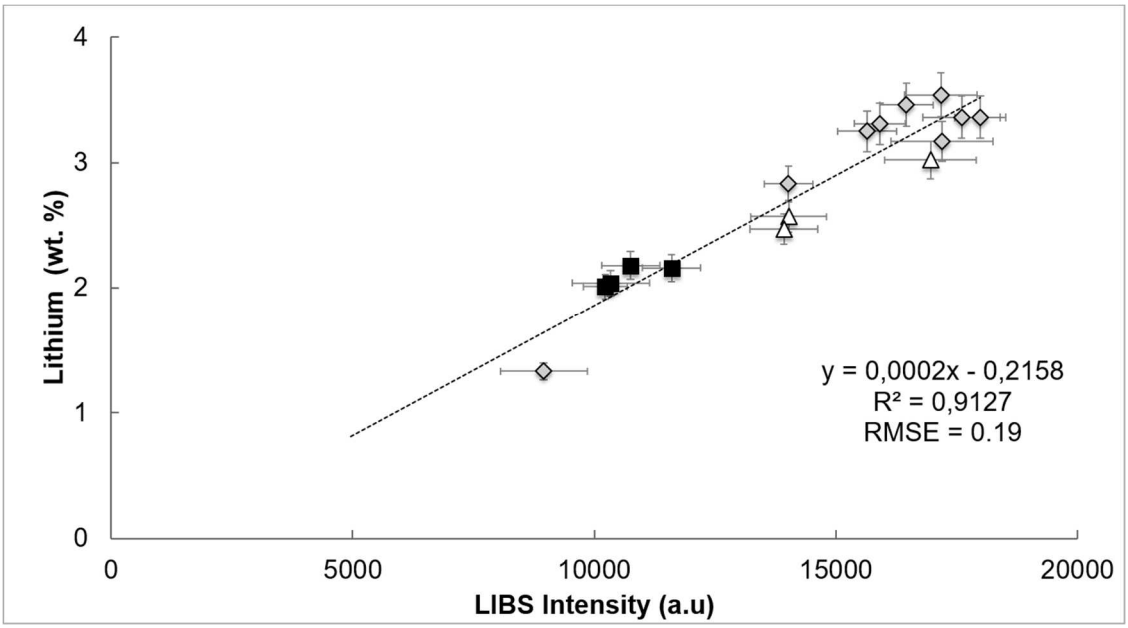

Fig. 3 Calibration curve obtained for the 16 Li-rich minerals. Error bars are shown for both the LIBS analyses and the Li bulk contents (AAS). Symbols: diamond for spodumene, triangle for lepidolite and square for petalite.

316 Part of the information that can be extracted from the LIBS handheld instrument and used for
317 development of the calibration curve is reported in Table 3. The relative standard deviation
318 (RSD) values obtained on the averaged Li emission line intensities are around 13%, can be
319 down to 9%, but generally do not exceed 18%. These variations have two possible causes.
320 The first is compositional heterogeneity within a sample, in that minerals may be
321 compositionally zoned in ways not observed by visual inspection but would be detected by the
322 LIBS analysis as the laser beam spot size on the sample is 50 µm. The second is a matrix effect
323 related to likely differences in the volume of sample ablated by each laser shot at the different
324 points along the two raster grids. Both of these potential complications have been addressed by
325 making 30 LIBS analyses at two places on each sample in order to obtain a pseudo-bulk analysis
326 that somewhat representative of the entire sample. As shown in Fig. 3, there is a high degree of
327 correlation, with R^2 >0.9 and RMSE-P = 0.19 wt. % for this Li mineral calibration. This means
328 that for each quantification of Li on new mineral, the error will be ± 0.19 wt. % Li, thus allowing
329 the discrimination of the mineral end-members and delivering very good Li quantification when
330 used in the field.
331
332 Table 3
333 Information from the Z-300 handheld LIBS analyzer used for the establishment of the Li
334 calibration curve. Li emission areas are reported as baseline corrected emission intensities in
335 arbitrary units (a.u.). RSD values are calculated for the 30 LIBS analyses of each mineral.
336 Reference Li contents (in wt. %) are from the independent analysis by flame AAS (5%). The
337 calculated Li contents are the values obtained from the LIBS calibration curve (Fig. 3).
338

Sample ID	Li Emission Intensity (a.u.)	RSD LIBS (%)	Reference Li Content (wt. %)	Error content (Li wt. %)	Calculated Li content (wt. %)
Spo-Zai	8952	17.6	1.33	0.06	1.64
Spo-Pak	17991	10.8	3.36	0.17	3.52
Spo-Nor	15648	11.3	3.25	0.16	3.03
Spo-Lac	14017	9.4	2.83	0.14	2.70
Spo-Kok	15908	10.8	3.31	0.16	3.09
Spo-Boa	16461	10.8	3.46	0.17	3.20
Spo-Big	17198	19.7	3.17	0.16	3.36
Pet-Tan	10751	11.6	2.18	0.11	2.02
Pet-Bik2	10337	15.4	2.04	0.10	1.93
Pet-Bik	11597	11.6	2.16	0.11	2.19

Pet-Big	10225	9.1	2.01	0.10	1.91
Lep-Pak	13923	13.8	2.47	0.12	2.68
Lep-Moz	14022	16.1	2.57	0.13	2.70
Lep-Cun	16959	18.1	3.02	0.15	3.31
Kun-Afg	17173	12.7	3.54	0.18	3.35
Hid-Afg	17603	14.3	3.36	0.17	3.44

339

340 *4.3 Discrimination of Li-bearing minerals*

341 Since LIBS has the potential of detecting most elements of the periodic table, it is common to
342 use LIBS analysis to discriminate mineral phases of similar composition (McMillan et al.,
343 2006; Harmon et al., 2009; Farnsworth-Pinkerton et al., 2018). This capability would be
344 especially useful during fieldwork, where it might be used to rapidly distinguish between Li
345 minerals of similar appearance but different major element composition, as is the case for
346 spodumene and petalite. Although these minerals are generally difficult to distinguish visually,
347 they are characterized by distinct Si and Al proportions and, therefore, have different Si/Al
348 ratios that can be observed in LIBS spectra. The diagrams of Fig. 4 show LIBS spectra between
349 287-311 nm for petalite, spodumene, and lepitolite, displaying the emission line for Si at 288.16
350 nm and the two emission lines for Al at 308.21 and 309.27 nm. The relative difference in peak
351 intensities between Al and Si results in a high Si/Al ratio for petalite and low ratios for
352 spodumene and lepidolite. Indeed, a rapid look at such spectra on the LIBS analyzer in the field
353 could help to quickly discriminate a mineral like petalite with a relatively high Si/Al ratio from
354 spodumene with a low Si/Al ratio. Similarly, it should be possible to distinguish between petalite
355 and spodumene according to the intensity K emission lines at 766.49 nm and 769.89 nm (not
356 visible here). Lepidolites can be easily identified in the field due to their purple color. This
357 capability to rapidly identify elements and element ratios for minerals in the field represents one
358 of the primary utilities of handheld LIBS instrument.

359

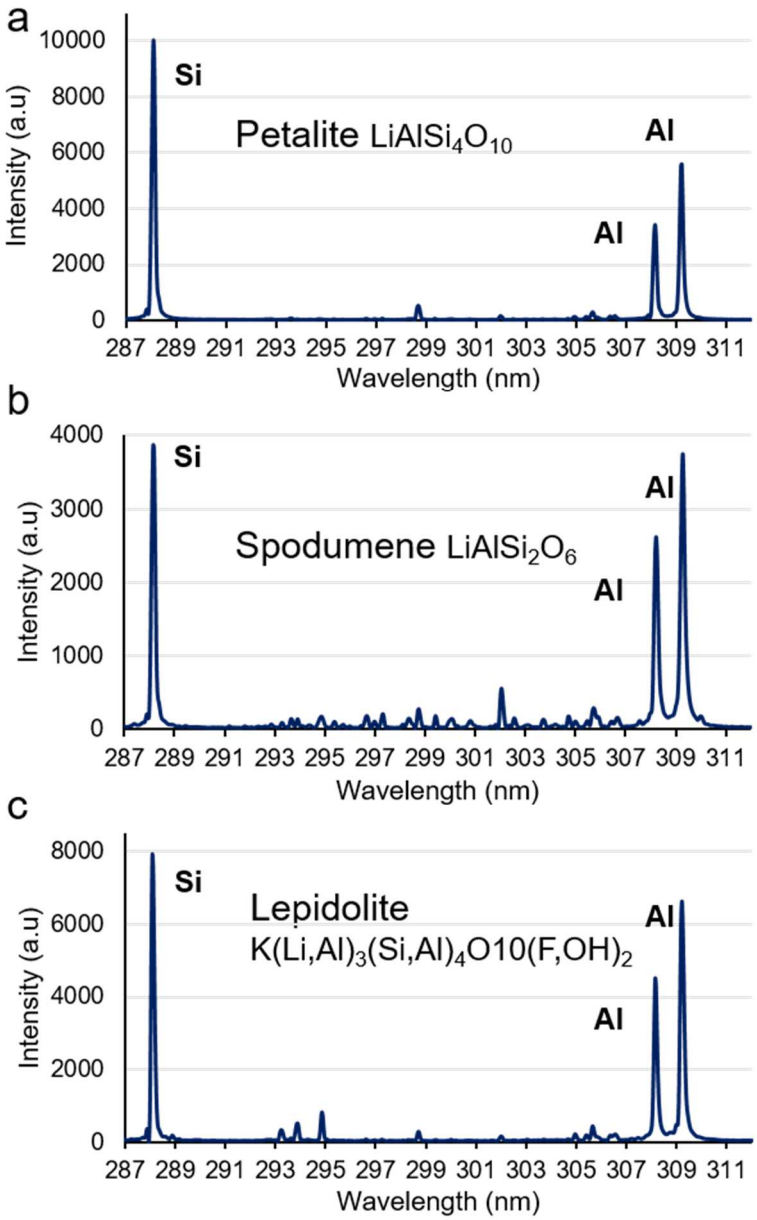

Fig. 4 Representative LIBS spectra between 287–311 nm, with intensities expressed in arbitrary units (a.u.), a) petalite, b) spodumene and c) lepidolite.

4.4 LIBS detection of trace elements

LIBS also has the potential to detect other light elements, such as Be, Rb and Cs, other rare metals that commonly occur in pegmatites along with Li. The detection of trace concentrations of such elements has important implications for Li exploration. Indeed, high Be, Rb, and Cs contents in muscovite micas can be used as indicator of Li-fertility, which permits discrimination between barren and Li-mineralized granites and pegmatites (Ballouard et al., 2020; Černý, 1989; Gordiyenko, 1971; Selway et al., 2005). Similarly, secondary or fluid-modified minerals, which result from the pervasive circulation of hydrothermal fluids that produces country-rock

aureoles of Li mineralization in metasomatized pegmatites and granites, can be strongly enriched in Li, Be, Rb, and Cs (Ballouard et al., 2020; Barros et al., 2020; Selway et al., 2005). Typically, such enrichment is the most pronounced in the first 10s of meters away from the country rocks surrounding mineralized intrusions. Li, Cs, and Rb concentrations in metasomatic biotite and muscovite at the intrusion-country rock contact can commonly be between 1000 ppm and 1 wt. % (Ballouard et al., 2020) with such anomalies sometimes extending outward for a distance of >1 km (Selway et al., 2005). Therefore, the direct measurement of trace and minor elements in micas using handled LIBS in the field can be a powerful tool for rare metal deposit exploration.

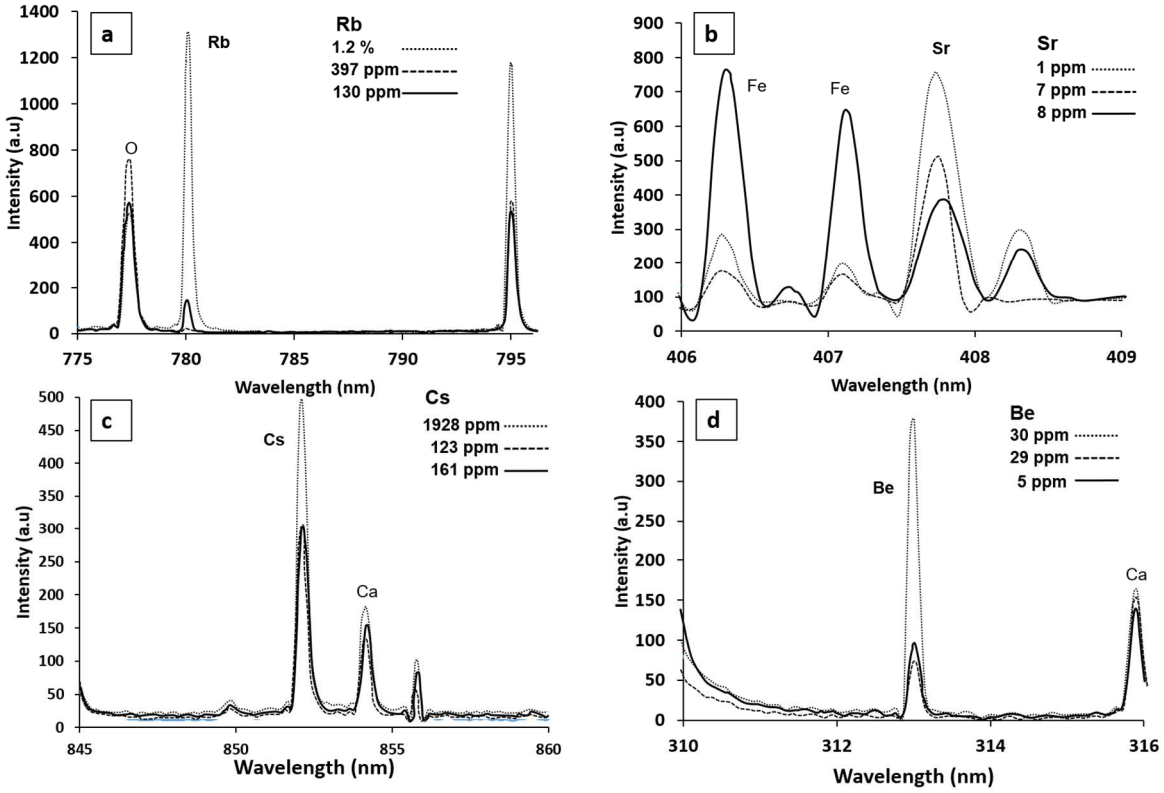

Fig. 5 LIBS spectra over selected wavelength intervals displaying Rb, Sr, Cs and Be most intensive emission lines. The fine dotted line denotes lepidolite, the dashed line denotes petalite and the solid line denotes spodumene. The LIBS spectra are averaged spectra obtained on the 30 points for each mineral and they are not normalized. The legend for each plot indicates the elemental concentrations for Rb, Sr, Cs and Be. a) spectra between 775-795 nm for Rb, b) spectra between 406-409 nm for Sr, c) spectra between 845-860 nm for Cs, d) spectra between 310-316 nm for Be.

The LIBS spectra shown in Fig. 5 are averaged spectra for each of the three Li minerals analyzed, i.e. the lepidolite profile is the average spectrum for the three lepidolite samples. Their

contents, obtained from the independent bulk analysis, testify that the limit of detection are in agreement with such low concentration. As these spectra are not normalized, it is not possible to directly compare emission intensities of the trace elements among the different minerals. According to these results, Be and Sr can be detected down to the ppm level, as previously observed for Li (0.1 ppm estimated), Rb can be detected down to 20 ppm, and the detection limit for Cs is estimated at around 15 ppm. These limits of detection for such low-abundance trace elements are in agreement to the concentrations commonly reported for such Li-minerals (Selway et al., 2005; Van Lichtervelde et al., 2008).

5. Discussion

The analytical approach followed for this work was developed around a number of interrogations, regarding the quite recent portable LIBS technology and its application to geological material. Qualitative LIBS analysis has been the focus of most previous studies due to high emissivity of atoms and ions in plasma conditions in reaction to the laser beams, and most importantly for the wide range of detection, from a few ppms to percentage concentration levels during the same analysis. These features are widely exploited, especially in the microchemical mapping of mineral surfaces and various materials. (Sweetapple and Tassios, 2015a; Kuhn et al., 2016; Fabre et al., 2018; Jolivet et al., 2019; Lawley et al., 2021). However, the quantitative aspect is still challenging because of both chemical and physical effects related to the type of material analyzed and the type of LIBS used (Rosenwasser et al., 2001; Sobron, 2019; Harmon and Senesi, 2021). Similarly to conventional analytical methods, standards with known physical and chemical properties have to be used to build predictive models and provide concentration estimates.

This study started by testing different analytical parameters in order to optimize the LIBS sample acquisition for the analyte and the samples to be tested. AS previously described, the optimized number of laser shots is dependent on the chemical homogeneity of the sample and the grain size of the sample in relation to the laser spot size. Regarding the size of the minerals, one should multiply the number of the laser shots to obtain a bulk composition. As the collection of spectra is fast, around 30s for each raster grid, the LIS analysis seems to be faster than for handheld XRF analyzers, with the option to directly control the LIBS spectra are attractive aspects for exploration purpose. Similarly, minimal sample preparation is also an advantage avoiding any use of powders or pressed pellets, that are sometimes required for quantitative analysis for other portable instrument such as XRF (Gazley and Fisher, 2014; Lemière and

Harmon, 2021). In addition to being able to use a priori compositional knowledge of the standards used for calibration, the portable LIBS instrument allows the analyst to define and compare different calibration tests while varying the spectra acquisition parameters (e.g. number of analysis points, number of laser shots, laser repetition rate, …etc.). The statistical parameters of RMSE-P (as displayed by error bars in the calibration curve of Fig. 3) and RSD, which are calculated by the internal software, are strong indicators regarding the accuracy of the analytical results and, consequently, the calibration model. For exploration context, this value of 0.19 wt% is sufficient to discriminate the different minerals and to provide a good estimate of the Li content. The use of handheld LIBS is of first interest to limit the sampling with the good identification of Li-bearing minerals and to limit the future chemical analyses.

The LIBS analyses were obtained on a single LIBS analyzer after internal wavelength calibration, with spectral pre- processing and processing performed with its onboard software. It is worth noting that LIBS spectra acquired can be used as raw data, i.e. without any treatment or correction, by exporting the data for external processing that gives the analyst more options to pre-process and process data according to the particular objectives of a study. Pre-processing of LIBS spectra was performed via the integrated software, which is an important capability for field use. For classical LIBS analysis, baseline and noise corrections are optional depending on evaluation by the analyst of the LIBS spectra and emission lines present for specific elements of interest. Normalization is also commonly used to attenuate the shot-to-shot fluctuations in laser energy and laser-sample interactions under the same acquisition protocol. Total area normalization was used for this study, as different types of Li minerals were analyzed. For our application, the normalization process only takes into account a potential chemical effect, considering that all samples analyzed are naturally-occurring mineral specimens (no grains or powders) and were subject to the same preparation.

The potential of LIBS for the detection and quantification of elements lighter than Mg is very important for geological purposes. No other technique is able to rapidly analyze these elements on unprepared samples. Hence, having such a capability in a handheld device is quite revolutionary for field geologists. The use of LIBS spectra for material discrimination is also a very useful field analysis capability, as it exploits abundance differences in detected elements to gain insight into a sample's mineralogy, which can be especially useful during the early stages of a mineral exploration and sampling campaign when the conventional macroscopic tests for mineral identification (e.g. luster, color, streak, hardness, cleavage) are difficult to

perform due to sample size, shape, or degree of alteration degree. Due to the small size of the laser spot, handheld LIBS can precisely analyze a small area of a sample of ~50μm diameter and detect a wide range of major, minor, and trace elements, which allows the analyst to correctly identify the sample's mineralogy through comparison against a pre-assembled library of spectra and/or element ratio. LIBS analysis is rapid and the internal software ranks detected elements according to their "percentage of likelihood", which is a parameter that the software determines by matching the emission lines detected lines in a spectrum of an element to an internal database derived from the NIST Atomic Spectra Database (Kramida et al., 2018) and then compares the intensity levels recorded for each line. This option was very useful for trace elements as shown in Fig. 5. The detection of high-Li with a high K-content can help the geologist to identify the lepidolite minerals in place. Elements such as Be, Rb, and Cs were detected in almost every analyzed mineral but usually with higher intensity levels in lepidolite than in petalite and spodumene. The bulk analyses not only confirmed the presence of these trace elements in the sample suite and documented that lepidolite was more enriched in Rb especially and then Be and Cs. Importantly, this highlights that samples with only a few 10s of ppm abundance of these trace elements could be detected by the handheld LIBS instrument.

6. Conclusions

Handheld LIBS is a powerful tool with a strong potential for both qualitative and quantitative analysis. More such case studies are needed to realize its advantages for field use. This study began with a focus on setting up the most appropriate LIBS analysis (multiplying the number of points) and data processing protocol (internal normalization) for a dataset obtained for a suite of 16 Li minerals comprised of three major mineral species (lepidolite, petalite and spodumene). Thus, the resulting calibration curve showed that LIBS data compared well with Li contents determined from conventional techniques with an RMSE of 0.19 wt. % Li. Although very encouraging, the results of this study for Li quantification should be validated through analysis of a larger collection of Li minerals. The discrimination aspect of LIBS is quite promising given its capability for major, minor, and trace element analysis, which allows the analyst more freedom in terms of element selection for discrimination depending on the particular characteristics of different sample types. For this study, the major elements Si, Al, and K were detected and their measured relative intensities can be used for mineral discrimination. The ratio between the Si and Al intensities can be observed to successfully discriminated petalite from spodumene and lepidolite (Fig. 4). It was proposed that a similar comparison of K intensity

comparison could be used to identify lepidolite. As is the situation with quantitative analysis, use of LIBS for mineral discrimination should also be designed for the specific mineralogy of the sample type being investigated and the particular elements associated with target ore minerals. Considering that trace elements occur in various amounts depending on geological setting, handheld LIBS analysis could be used to discriminate mineral species of interest. Calibration curves can be developed for LIBS data from a portable device rapidly and efficiently, with its use in an exploration program able to provide a considerable time and cost saving.

Funding: This research was funded by the ERA-MIN/0001/2017–LIGHTS project. This work was also supported by the French National Research Agency through the national program "Investissements d'avenir" with the reference ANR-10-LABX-21 - RESSOURCES21.

Author contributions:

Nour Eddine Ourti: Conceptualization, methodology, validation, formal analysis, writing-original draft preparation, writing-review editing

Cécile Fabre: Conceptualization, methodology, validation, formal analysis, investigation, data curation, writing-original draft preparation, writing-review editing, visualization, supervision

Christophe Ballouard: Conceptualization, methodology, writing-original draft preparation

Jean Cauzid: Conceptualization, methodology, supervision, writing-review editing, project administration, funding acquisition

Julien Mercadier: methodology

Acknowledgments: We acknowledge Robert Linnen, Tania Martin and Marc Binnen and the Suffel Collection, department of Ontario, for providing some of the Li-rich minerals and SciAps Company for technical information. We warmly thank R. Harmon for his kind review, and his expertise, as well as the second anonymous reviewer. They have greatly contributed to the improvement of this manuscript.

Babos, D.V., Barros, A.I., Nóbrega, J.A., Pereira-Filho, E.R., 2019. Calibration strategies to overcome matrix effects in laser-induced breakdown spectroscopy: Direct calcium and phosphorus determination in solid mineral supplements. Spectrochimica Acta Part B: Atomic Spectroscopy 155, 90–98. https://doi.org/10.1016/j.sab.2019.03.010

Ballouard, C., Elburg, M.A., Tappe, S., Reinke, C., Ueckermann, H., Doggart, S., 2020. Magmatic-hydrothermal evolution of rare metal pegmatites from the Mesoproterozoic Orange River pegmatite belt (Namaqualand, South Africa). Ore Geology Reviews 116, 103252. https://doi.org/10.1016/j.oregeorev.2019.103252

Barros, R., Kaeter, D., Menuge, J.F., Škoda, R., 2020. Controls on chemical evolution and rare element enrichment in crystallising albite-spodumene pegmatite and wallrocks: Constraints from mineral chemistry. Lithos 352–353, 105289. https://doi.org/10.1016/j.lithos.2019.105289

Bennett, B.N., Martin, M.Z., Leonard, D.N., Garlea, E., 2018. Calibration curves for commercial copper and aluminum alloys using handheld laser-induced breakdown spectroscopy. Appl. Phys. B 124, 42. https://doi.org/10.1007/s00340-018-6909-x

Bibienne, T., Magnan, J.-F., Rupp, A., Laroche, N., 2020. From Mine to Mind and Mobiles: Society's Increasing Dependence on Lithium. Elements 16, 265–270. https://doi.org/10.2138/gselements.16.4.265

Bowell, R.J., Lagos, L., de los Hoyos, C.R., Declercq, J., 2020. Classification and Characteristics of Natural Lithium Resources. Elements 16, 259–264. https://doi.org/10.2138/gselements.16.4.259

Černý, P., 1991. Rare-element Granitic Pegmatites. Part I: Anatomy and Internal Evolution of Pegmatite Deposits. Geoscience Canada 18(2), 49–67.

Černý, P., 1989. Exploration Strategy and Methods for Pegmatite Deposits of Tantalum, in: Möller, P., Černý, Petr, Saupé, F. (Eds.), Lanthanides, Tantalum and Niobium, Special Publication No. 7 of the Society for Geology Applied to Mineral Deposits. Springer, Berlin, Heidelberg, pp. 274–302. https://doi.org/10.1007/978-3-642-87262-4_13

Charoy, B., Chaussidon, M., Noronha, F., 1995. Lithium zonation in white micas from the Argemela microgranite (central Portugal): an in-situ ion-, electron-microprobe and spectroscopic investigation. European Journal of Mineralogy 335–352. https://doi.org/10.1127/ejm/7/2/0335

Connors, B., Somers, A., Day, D., 2016. Application of Handheld Laser-Induced Breakdown Spectroscopy (LIBS) to Geochemical Analysis. Appl Spectrosc 70, 810–815. https://doi.org/10.1177/0003702816638247

Cremers, D.A., Radziemski, L.J., 2006. History and fundamentals of LIBS, in: Laser Induced Breakdown Spectroscopy: Fundamentals and Applications. Cambridge University Press, pp. 9–16.

Cuñat, J., Palanco, S., Carrasco, F., Simón, M.D., Laserna, J.J., 2005. Portable instrument and analytical method using laser-induced breakdown spectrometry for in situ characterization of speleothems in karstic caves. J. Anal. At. Spectrom. 20, 295–300. https://doi.org/10.1039/B417161F

Defnet, P.A., Wise, M.A., Harmon, R.S., Hark, R.R., Hilferding, K., 2021. Analysis of Garnet by Laser-Induced Breakdown Spectroscopy—Two Practical Applications. Minerals 11, 705. https://doi.org/10.3390/min11070705

Duponchel, L., Bousquet, B., Pelascini, F., Motto-Ros, V., 2020. Should we prefer inverse models in quantitative LIBS analysis? J. Anal. At. Spectrom. 35, 794–803. https://doi.org/10.1039/C9JA00435A

El Haddad, J., Canioni, L., Bousquet, B., 2014. Good practices in LIBS analysis: Review and advices. Spectrochimica Acta Part B: Atomic Spectroscopy 101, 171–182. https://doi.org/10.1016/j.sab.2014.08.039

574 Fabre, C., 2020. Advances in Laser-Induced Breakdown Spectroscopy analysis for geology: A
575 critical review. Spectrochimica Acta Part B: Atomic Spectroscopy 166, 105799.
576 https://doi.org/10.1016/j.sab.2020.105799
577 Fabre, C., Boiron, M.-C., Dubessy, J., Chabiron, A., Charoy, B., Martin Crespo, T., 2002.
578 Advances in lithium analysis in solids by means of laser-induced breakdown
579 spectroscopy: an exploratory study. Geochimica et Cosmochimica Acta 66, 1401–
580 1407. https://doi.org/10.1016/S0016-7037(01)00858-4
581 Fabre, C., Boiron, M.-C., Dubessy, J., Moissette, A., 1999. Determination of ions in individual
582 fluid inclusions by laser ablation optical emission spectroscopy: development and
583 applications to natural fluid inclusions. Journal of Analytical Atomic Spectrometry 14,
584 913–922. https://doi.org/10.1039/a809338e
585 Fabre, C., Cousin, A., Wiens, R.C., Ollila, A., Gasnault, O., Maurice, S., Sautter, V., Forni, O.,
586 Lasue, J., Tokar, R., Vaniman, D., Melikechi, N., 2014. In situ calibration using
587 univariate analyses based on the onboard ChemCam targets: first prediction of
588 Martian rock and soil compositions. Spectrochimica Acta Part B: Atomic Spectroscopy
589 99, 34–51. https://doi.org/10.1016/j.sab.2014.03.014
590 Fabre, C., Maurice, S., Cousin, A., Wiens, R.C., Forni, O., Sautter, V., Guillaume, D., 2011.
591 Onboard calibration igneous targets for the Mars Science Laboratory Curiosity rover
592 and the Chemistry Camera laser induced breakdown spectroscopy instrument.
593 Spectrochimica Acta Part B: Atomic Spectroscopy 66, 280–289.
594 https://doi.org/10.1016/j.sab.2011.03.012
595 Fabre, C., Ourti, N.E., Mercadier, J., Cardoso-Fernandes, J., Dias, F., Perrotta, M., Koerting, F.,
596 Lima, A., Kaestner, F., Koellner, N., Linnen, R., Benn, D., Martins, T., Cauzid, J., 2021.
597 Analyses of Li-Rich Minerals Using Handheld LIBS Tool. Data 6, 68.
598 https://doi.org/10.3390/data6060068
599 Gazley, M., Fisher, L., 2014. A review of the reliability and validity of portable X-ray
600 fluorescence spectrometry (pXRF) data. pp. 69–82.
601 Gordiyenko, V.V., 1971. Concentrations of Li, Rb, and Cs in potash feldspar and muscovite as
602 criteria for assessing the rare-metal mineralization in granite pegmatites.
603 International Geology Review 13, 134–142.
604 https://doi.org/10.1080/00206817109475411
605 Gourcerol, B., Gloaguen, E., Melleton, J., Tuduri, J., Galiegue, X., 2019. Re-assessing the
606 European lithium resource potential – A review of hard-rock resources and
607 metallogeny. Ore Geology Reviews 109, 494–519.
608 https://doi.org/10.1016/j.oregeorev.2019.04.015
609 Grew, E.S., 2020. The Minerals of Lithium. Elements 16, 235–240.
610 https://doi.org/10.2138/gselements.16.4.235
611 Guezenoc, J., Gallet-Budynek, A., Bousquet, B., 2019a. Critical review and advices on
612 spectral-based normalization methods for LIBS quantitative analysis. Spectrochimica
613 Acta Part B: Atomic Spectroscopy 160, 105688.
614 https://doi.org/10.1016/j.sab.2019.105688
615 Guezenoc, J., Payré, V., Fabre, C., Syvilay, D., Cousin, A., Gallet-Budynek, A., Bousquet, B.,
616 2019b. Variable selection in laser-induced breakdown spectroscopy assisted by
617 multivariate analysis: An alternative to multi-peak fitting. Spectrochimica Acta Part B:
618 Atomic Spectroscopy 152, 6–13. https://doi.org/10.1016/j.sab.2018.12.001
619 Hahn, D.W., Omenetto, N., n.d. Laser-Induced Breakdown Spectroscopy (LIBS), Part II:
620 Review of Instrumental and Methodological Approaches to Material Analysis and

621 Applications to Different Fields [WWW Document]. ResearchGate. URL
622 https://www.researchgate.net/publication/221981551_Laser-
623 Induced_Breakdown_Spectroscopy_LIBS_Part_II_Review_of_Instrumental_and_Met
624 hodological_Approaches_to_Material_Analysis_and_Applications_to_Different_Field
625 s (accessed 8.8.19).
626 Harmon, Lawley, Watts, Harraden, Somers, Hark, 2019. Laser-Induced Breakdown
627 Spectroscopy—An Emerging Analytical Tool for Mineral Exploration. Minerals 9, 718.
628 https://doi.org/10.3390/min9120718
629 Harmon, R.S., DeLucia, F.C., McManus, C.E., McMillan, N.J., Jenkins, T.F., Walsh, M.E.,
630 Miziolek, A., 2006. Laser-induced breakdown spectroscopy – An emerging chemical
631 sensor technology for real-time field-portable, geochemical, mineralogical, and
632 environmental applications. Applied Geochemistry 21, 730–747.
633 https://doi.org/10.1016/j.apgeochem.2006.02.003
634 Harmon, R.S., Khashchevskaya, D., Morency, M., Owen, L.A., Jennings, M., Knott, J.R.,
635 Dortch, J.M., 2021. Analysis of Rock Varnish from the Mojave Desert by Handheld
636 Laser-Induced Breakdown Spectroscopy. Molecules 26, 5200.
637 https://doi.org/10.3390/molecules26175200
638 Harmon, R.S., Remus, J., McMillan, N.J., McManus, C., Collins, L., Gottfried, J.L., DeLucia, F.C.,
639 Miziolek, A.W., 2009. LIBS analysis of geomaterials: Geochemical fingerprinting for
640 the rapid analysis and discrimination of minerals. Applied Geochemistry 24, 1125–
641 1141. https://doi.org/10.1016/j.apgeochem.2009.02.009
642 Harmon, R.S., Senesi, G.S., 2021. Laser-Induced Breakdown Spectroscopy – A geochemical
643 tool for the 21st century. Applied Geochemistry 128, 104929.
644 https://doi.org/10.1016/j.apgeochem.2021.104929
645 Kesler, S.E., Gruber, P.W., Medina, P.A., Keoleian, G.A., Everson, M.P., Wallington, T.J., 2012.
646 Global lithium resources: Relative importance of pegmatite, brine and other deposits.
647 Ore Geology Reviews 48, 55–69. https://doi.org/10.1016/j.oregeorev.2012.05.006
648 Kochelek, K.A., McMillan, N.J., McManus, C.E., Daniel, D.L., 2015. Provenance determination
649 of sapphires and rubies using laser-induced breakdown spectroscopy and
650 multivariate analysis. American Mineralogist 100, 1921–1931.
651 https://doi.org/10.2138/am-2015-5185
652 Kramida, A., Ralchenko, Y., Reader, J., 2018. NIST Atomic Spectra Database (Version 5.5.6) ;
653 National Institute of Standards and Technology: Gaithersburg, MD, USA. Available :
654 https://physics.nist.gov/asd.
655 Lawley, C.J.M., Somers, A.M., Kjarsgaard, B.A., 2021. Rapid geochemical imaging of rocks and
656 minerals with handheld laser induced breakdown spectroscopy (LIBS). Journal of
657 Geochemical Exploration 222, 106694. https://doi.org/10.1016/j.gexplo.2020.106694
658 Lemière, B., Harmon, R.S., 2021. XRF and LIBS for Field Geology, in: Portable Spectroscopy
659 and Spectrometry. John Wiley & Sons, Ltd, pp. 455–497.
660 https://doi.org/10.1002/9781119636489.ch42
661 Linnen, R.L., Van Lichtervelde, M., Cerny, P., 2012. Granitic Pegmatites as Sources of
662 Strategic Metals. Elements 8, 275–280. https://doi.org/10.2113/gselements.8.4.275
663 London, D., 2014. A petrologic assessment of internal zonation in granitic pegmatites. Lithos
664 184–187, 74–104. https://doi.org/10.1016/j.lithos.2013.10.025
665 London, D., 2005a. Granitic pegmatites: an assessment of current concepts and directions
666 for the future. Lithos 80, 281–303. https://doi.org/10.1016/j.lithos.2004.02.009

London, D., 2005b. Granitic pegmatites: an assessment of current concepts and directions for the future. Lithos, Granitic Systems 80, 281–303. https://doi.org/10.1016/j.lithos.2004.02.009

London, D., 1984. Experimental phase equilibria in the system LiAlSiO4–SiO2–H2O: a petrogenetic grid for lithiumx-rich pegmatites. American Mineralogist 69, 995–1004.

McMillan, N.J., Curry, J., Dutrow, B.L., Henry, D.J., 2018. Identification of the Host Lithology of Tourmaline Using Laser-Induced Breakdown Spectroscopy For Application in Sediment Provenance and Mineral Exploration. The Canadian Mineralogist 56, 393–410. https://doi.org/10.3749/canmin.1800004

Palanco, S., Alises, A., Cuñat, J., Baena, J., Laserna, J.J., 2003. Development of a portable laser-induced plasma spectrometer with fully-automated operation and quantitative analysis capabilities. J. Anal. At. Spectrom. 18, 933–938. https://doi.org/10.1039/B303248E

Radziemski, L., Cremers, D., 2013. A brief history of laser-induced breakdown spectroscopy: From the concept of atoms to LIBS 2012. Spectrochimica Acta Part B: Atomic Spectroscopy 87, 3–10. https://doi.org/10.1016/j.sab.2013.05.013

Rakovský, J., Čermák, P., Musset, O., Veis, P., 2014. A review of the development of portable laser induced breakdown spectroscopy and its applications. Spectrochimica Acta Part B: Atomic Spectroscopy 101, 269–287. https://doi.org/10.1016/j.sab.2014.09.015

Rossi, M., Dell'Aglio, M., De Giacomo, A., Gaudiuso, R., Senesi, G.S., De Pascale, O., Capitelli, F., Nestola, F., Ghiara, M.R., 2014. Multi-methodological investigation of kunzite, hiddenite, alexandrite, elbaite and topaz, based on laser-induced breakdown spectroscopy and conventional analytical techniques for supporting mineralogical characterization. Phys Chem Minerals 41, 127–140. https://doi.org/10.1007/s00269-013-0631-3

Selway, J.B., Breaks, F.W., Tindle, A.G., 2005. A review of rare-element (Li-Cs-Ta) pegmatite exploration techniques for the Superior Province, Canada, and large worldwide tantalum deposits. Exploration and Mining Geology 14, 1–30.

Senesi, G.S., 2014. Laser-Induced Breakdown Spectroscopy (LIBS) applied to terrestrial and extraterrestrial analogue geomaterials with emphasis to minerals and rocks. Earth-Science Reviews 139, 231–267. https://doi.org/10.1016/j.earscirev.2014.09.008

Senesi, G.S., Harmon, R.S., Hark, R.R., 2021. Field-portable and handheld laser-induced breakdown spectroscopy: Historical review, current status and future prospects. Spectrochimica Acta Part B: Atomic Spectroscopy 175, 106013. https://doi.org/10.1016/j.sab.2020.106013

Sweetapple, M.T., Tassios, S., 2015. Laser-induced breakdown spectroscopy (LIBS) as a tool for in situ mapping and textural interpretation of lithium in pegmatite minerals. American Mineralogist 100, 2141–2151. https://doi.org/10.2138/am-2015-5165

Tadesse, B., Makuei, F., Albijanic, B., Dyer, L., 2019. The beneficiation of lithium minerals from hard rock ores: A review. Minerals Engineering 131, 170–184. https://doi.org/10.1016/j.mineng.2018.11.023

Takahashi, H., Murano, T., Takakura, M., Asahina, S., Terauchi, M., Koike, M., Imazono, T., Koeda, M., Nagano, T., 2015. Development of soft X-ray emission spectrometer for EPMA/SEM and its application. Materials Science and Engineering 12.

Van Lichtervelde, M., Grégoire, M., Linnen, R.L., Béziat, D., Salvi, S., 2008. Trace element geochemistry by laser ablation ICP-MS of micas associated with Ta mineralization in

713 the Tanco pegmatite, Manitoba, Canada. Contrib Mineral Petrol 155, 791–806.
714 https://doi.org/10.1007/s00410-007-0271-z
715 Verlaguet, A., Brunet, F., Goffé, B., Menut, D., Findling, N., Poinssot, C., Huet, B., 2016.
716 Selective transfer of Li-Al-rich phyllosilicate to metamorphic veins (Western Alps):
717 Laser Induced Breakdown Spectroscopy (LIBS) compositional profiles and
718 microstructural characterization. Journal of Geodynamics 101, 51–72.
719 https://doi.org/10.1016/j.jog.2016.05.011
720 Zorov, N., Gorbatenko, A., Labutin, T., Popov, A., 2010. A review of normalization techniques
721 in analytical atomic spectrometry with laser sampling: From single to multivariate
722 correction. Spectrochimica Acta Part B: Atomic Spectroscopy 65, 642–657.
723 https://doi.org/10.1016/j.sab.2010.04.009
724